Chapter–4

Multifunctional biomass fuelled stove with provision of waste heat recovery

Chapter 4

Multifunctional biomass fuelled stove with provision of waste heat recovery

4.1 Introduction

Improvement of performance of biomass cook stove along with provision for its multifunctional feature are desired as discussed in the Chapter 1 and Chapter 2 in details. The attempts made so far to address these two issues are also presented and discussed in details in Chapter 2. The estimation of different components of heat, precisely delineated through heat transfer models, enables to identify potential options of performance improvement (Chapter 3). Waste heat recovery is a viable solution to improve performance of any thermal conversion devices [1-4]. However, option of waste heat utilization for efficiency improvement remains limited in biomass cook stove till now. Further, acceptability of the existing designs of multifunctional stoves [5-9] is also limited primarily due to users' inconveniences. It is realised that new design of cook stoves should focus on elements of improved combustion, air pre-heating and reduced emissions along with better efficiency [10-12] without compromising stability and portability of stoves [13]. Therefore, attempt is made to develop a new design of multifunctional improved cook stove integrating the desired features including waste heat recovery.

The present Chapter presents (i) the design concept, (ii) heat transfer analysis and prediction of performance and (iii) development and testing of the improved multifunctional biomass fuelled stove.

4.2 Methodology

The methodology used for development of the multifunctional biomass fuelled stove comprises of (i) development of conceptual design, (ii) prediction of performance using heat transfer analysis and (iii) development of prototype and testing which are discussed below.

4.2.1 Multifunctional improved biomass fuelled stove: concept and layout design

As discussed before additional features are conceptualized (i) to improve combustion, (ii) to utilize waste heat (iii) to minimize heat loss and (iii) to increase users'

convenience including additional applications. The details of the conceptualized features are presented in Table 4.1 and discussed below.

Table 4.1: Concept development and implementation strategy

Sl. No.	Concept	Feature	Performance indicators	Users' benefits
1.	Regulated air supply	Use of forced draft	• Enhances combustion • Increases efficiency • Enables optimum flame temperature	• Better regulation of power output
			• Reduces unburned fuel	• Reduces fuel consumption
2.	Provision of secondary air supply	Use of distributed plate	• Prevent unburned emissions	• Cleaner cooking
		Provision of cavity to hold fuel at the bottom half of the combustion chamber	• Reduces unburned fuel	• Faster cooking
			• Quicker ignition • Prevent unburned emissions	• Cleaner cooking
3.	Recovery of waste heat	Use of counter flow heat exchangers to recover heat from flame, flue gas and body of stove	• Enhances efficiency due to use of pre-heated air	• Reduces fuel consumption
			• Inclusion of more outlets for additional pots	• More cooking options
				• Space heating, baking, drying
4.	Minimize heat loss	Reduce thermal mass of the stove using modular design	• Enhances efficiency	• Reduces fuel consumption
		Use of a pot envelop to increase area of heat transfer and stability of the cooking pot	• Enhances efficiency by preventing radiation heat loss from flame	• Quicker cooking • Reduces fuel consumption
		Maximizing heat transfer from flame to pot by innovative design of combustion chamber	• Enhances efficiency by preventing radiation heat loss from flame	• Quicker cooking • Reduces fuel consumption
		Use of annular space to ensure primary and secondary air heating taking heat from combustion chamber outer wall	• Enhances efficiency by reducing skin heat loss and enhancing combustion efficiency	• Reduces fuel consumption
5.	Multifunctional and multiple pot applications	Use of high thermal conductivity metal plate for extracting heat from flue gas	• Enhance thermal efficiency, facilitate more options of uses	• Multiple pot cooking • Multiple functions
6.	Durability	Metallic body	• Increased durability • Reduction of thermal mass	• Attractive look • Faster cooking
7.	Portability and stability	Provisions of handles and supporting legs	• Portability • Stability	• Convenient handling

Sl. No.	Concept	Feature	Performance indicators	Users' benefits
8.	Uninterrupted use	Feed door for continuous feeding Ash tray for periodic ash removal	• Facilitate prolonged cooking	• Cleaner cooking • Faster cooking

Regulated power supply

Regulating the air supply through a fan run by auxiliary power is aimed for better combustion and thermal efficiency. The flame temperature could be varied according to user's cooking need and helping the users to regulate power output. Further, forced air reduces the unburned charcoal formation and thus prevents loss and expected to reduce fuel consumption.

Provision for secondary air supply

The provision for secondary air supply could be obtained using a distributor plate where the secondary air passes through top half to near pot bottom. This will reduce unburned emissions and cleaner cooking operation. The bottom half is exposed to primary air which holds the hot fuel bed and enables quicker ignition of fresh feed. This reduces the unburned fuel and prevents formation of unburned emissions which results in faster and cleaner cooking.

Recovery of waste heat

The stove should use heat exchangers to recover waste heat of flue gas and thermal body of the stove for processes such as preheating air and multifunctional or multiple pot applications. This is enable the users to have net reduction in fuel consumption, higher cooking options and enjoy other facilities of space heating, baking and drying.

Minimize heat loss

The overall heat loss minimization through reduction in thermal mass, use of pot skirt, maximizing flame to pot exposure area and using skin heat would improve the performance of the stove. A modular design of stove with pot envelope and well-designed combustion chamber enabling flame height for maximum pot contact area and reduction in its (combustion chamber) skin loss will enable reduction in fuel consumption and quicker cooking.

Multifunctional and multiple pot applications

Heat from the flue gas could be used by use of a high thermal conductivity metal plate for providing platform for multiple pot cooking and multifunction. This increases the uses and efficiency of the stove.

Durability, portability and stability

The stove should have a metallic body with handles and legs for higher durability, portability and stability. Metallic stoves have a lower thermal mass which enhances look and lowers cooking duration. The handles and legs increase the convenience in handling and provides support to the stove body.

Uninterrupted use

Use of feed door and ash tray will enable continuous cooking for longer cooking durations. The problems of fire chocking due to accumulation of ash on grate due to continuous feeding will be reduced with the use of ash tray. As a result flow of air will be continuous without hampering combustion and efficiency.

Finally, specific components are designed corresponding to the concepts discussed above for integration and subsequent analysis and testing of the multifunctional biomass fuelled stove as discussed below.

4.2.2 Development of multifunctional biomass fuelled stove

The entire scheme of the multifunctional stove is presented in Fig 4.1, 4.2 and 4.3 showing 38 components which is listed in Appendix E. The dimensions of the components are estimated (Fig. 4.8) using standard relationship and discussed in subsequent sections later in this Chapter.

Combustion chamber assembly

Overall, the stove is designed in two detachable sections where the lower section marked as stove which houses the combustion chamber. The connected upper section (upper chamber) is an assembly of heat exchangers to recover heat from flue gas and also to preheat air (described in details later). The open top combustion chamber is provided with a grate at its bottom where a portion of the rim is made perforated to pass

secondary air for combustion. A pot stand is also provided at the top rim to accommodate pots of standard sizes. One side (front side) of the cylindrical body of the stove is provided with rectangular opening with door for feeding fuel. The positioning of feed door is designed in such a way that during operation of stove the fuel would be directly placed in the hot zone of combustion chamber facilitating quicker ignition of fuel. A removable hinged ash tray beneath fuel grate of combustion chamber is designed in such a way that primary air can collect or abstract heat from the hot ash collected in ash tray before its (ash) disposal.

Further, lower section i.e., combustion chamber is surrounded by a rectangular outer cover forming an annular space around it to recover skin heat from the outer surface of the combustion chamber to preheat air. A horizontal plate at half of the height of the combustion chamber divides the annular space into two parts for heating primary and secondary air separately.

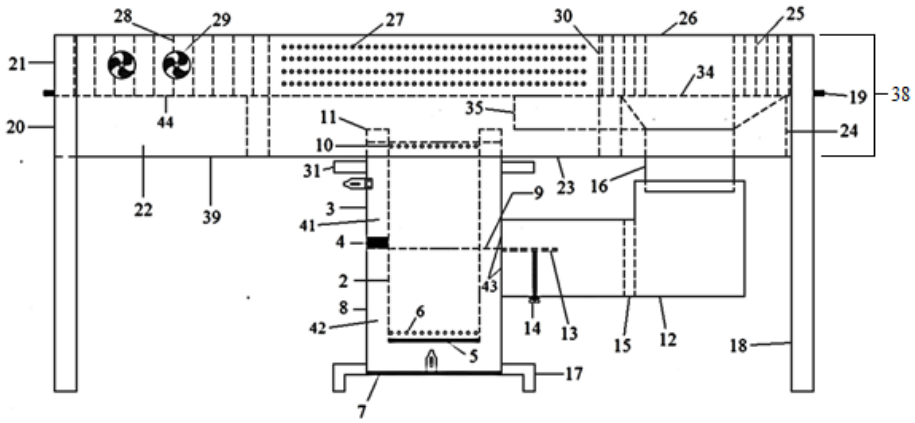

(a)

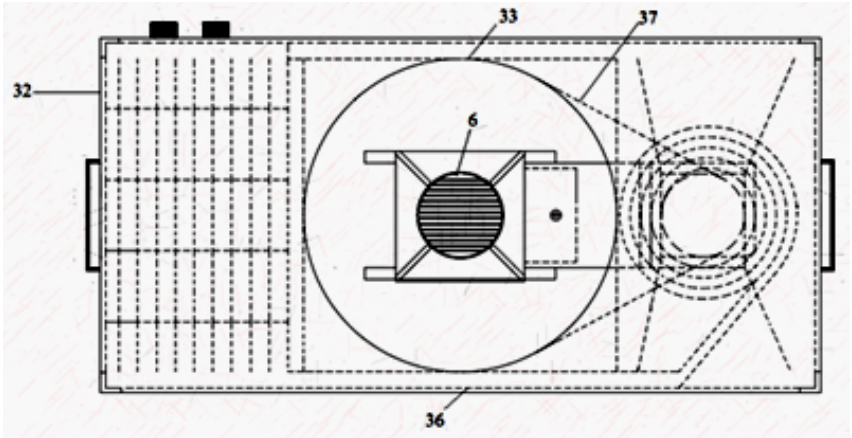

(b)

Fig.4.1: Multifunctional biomass fuelled stove (a) Front view (b) Top view, parts as shown in Table E.1 of Appendix E [24]

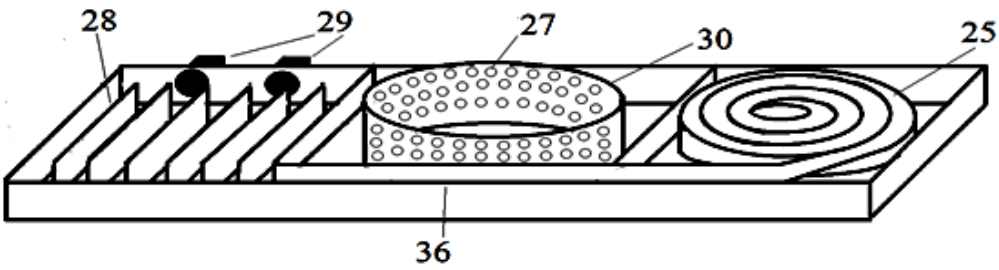

(a)

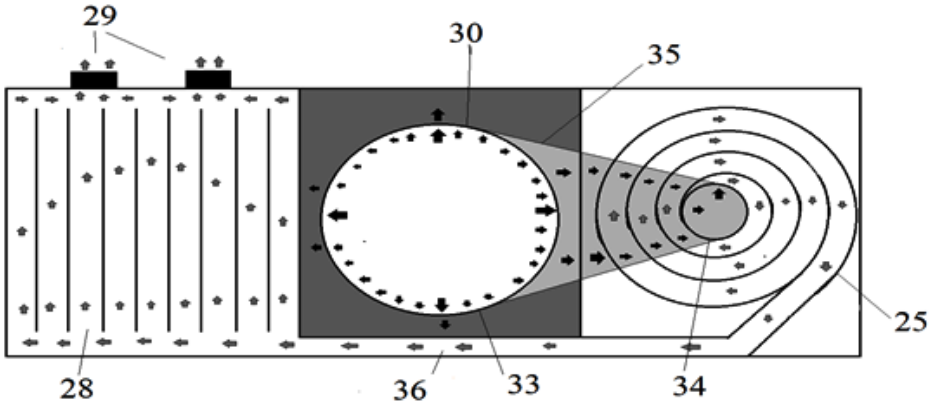

(b)

Fig.4.2: Assembly inside upper chamber (a) Flue gas heat extractors (b) Flue gas flow path inside flue gas heat extractors with parts listed in Table E.1 of Appendix E [24]

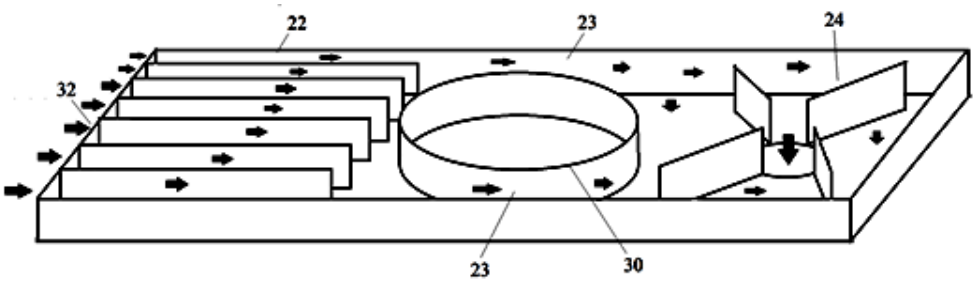

(a)

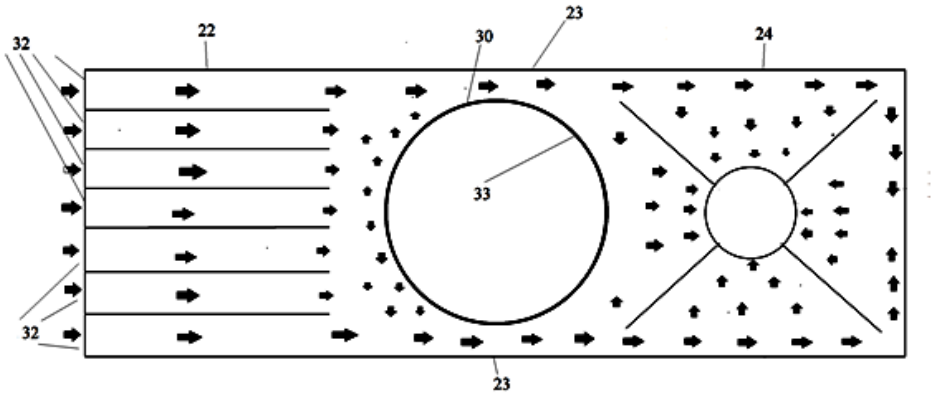

(b)

Fig.4.3: Assembly inside upper chamber (a) Air pre-heaters (radial flow air pre-heater: right side, and parallel flow air pre-heater: left side) (b) Pre-heated air flow path inside air pre-heaters with parts listed in Table E.1 of Appendix E [24]

Heat exchanger assembly

The upper section of the stove as mentioned earlier consists of two separate heat exchanger arrangements viz., (i) flue gas heat extractor and (ii) air pre-heater, former over that later. A parallel flow heat extractor (PHE) in one side and another spiral flow heat extractor (SHE) in another side comprise the top flue gas heat extractor as shown in Fig. 4.2. The flue gas from the combustion chamber enters SHE and after transferring heat to the top plate and to the bottom air pre-heater passed towards PHE before finally inducted by induced fans connected at the outlets provided with the PHE (Fig. 4.2). Reheating of the flue gas is achieved in between the two heat extractors by fresh flue gas while passing through a rectangular duct. A top detachable conducting plate covers both the heat extractors which also provides opening for accommodating the cooking pot. The conducting plate assists in multifunctional applications including cooking, space heating, drying and baking as per need.

Another rectangular plate separates the flue gas heat extractor from the air pre-heater located at its bottom. Air preheater located at the bottom of the flue gas heat extractor has also two separate sections at two ends viz., parallel flow air pre-heater (PAH) and radial flow air pre-heater (RAH) through which ambient air is sucked by an inline fan located inside the rectangular duct. The flow paths of air and flue gas are counter flow, ensuring proper heat transfer from flue gas to air (Fig. 4.3) at three phases viz, (i) PAH, (ii) connector between PAH and RAH and (iii) RAH. The pre-heated air is finally distributed into two parts by the distributor plate (primary combustion air through grate and secondary combustion air towards flame) for combustion.

A cylindrical ring extending from top of combustion chamber up to top of heat exchanger assembly located at center facilitates accommodation of primary pot. The ring has perforations at upper portion which is exposed to the flue gas heat extractor to facilitate flow of flue gas towards SHE. An annular gap between the pot and the ring is expected for required circulation of flue gas.

4.2.3 Methodology of design parameters

The designed features conceptualized and discussed in Section 4.2.1 and Table 4.1 to derive the benefits of waste heat recovery and multi-functionality along with enhancing

users convenience is attempted to be implemented as discussed above. It is expected that the desired performance of the cook stove will also enhance.

The determination of different design parameters requires a detailed analysis consisting of the standard protocol and heat transfer analysis. The methods followed for present research for determining key design parameters are presented below. Diameter of combustion chamber is dependent on dimension of cooking pot which in turn dependent on power output. Standard BIS methodology is used to estimate the diameter, height and expected thermal load of cooking pot.

The characteristics of fuel in terms of certain specific parameters (fuel particle dimension, elemental components of fuel, moisture content, heat content and density) is required to determine (i) flame characteristics (temperature, thickness, emissivity and ignition front velocity), (ii) air flow rate, (iii) flue gas flow rate. This is useful for designing of combustion chamber, heat exchangers, load capacity as well as fan size. Flame temperature is used for material and thickness selection. Height of combustion chamber is also estimated from dimension of flame which is a function of output power and fuel properties.

The heat exchanger assembly comprising of SHE, PHE, PAH and RAH as discussed above is designed based on expected quantity of heat estimated from heat transfer analysis and functional area requirement of stove surface area (Eq. 4.17, Eq. 4.18, Eq. 4.24 and Eq. 4.25).

Combustion chamber and fuel bed characteristics

Preliminary determination of combustion chamber dimensions could be determined using Eq. 4.1 from pot radius (r_p), gap height (H_g) and flame height (H_f). The flame height (H_f) further depends on power requirement (Q) and combustion chamber diameter ($D_{i,cc}$) as in Eq. 4.2 [15]. The combustion chamber diameter shows the particle distribution along the cross-section of the combustion chamber. The number of particles (n_p) and gaps (n_g) as in Eq. 4.3 and Eq. 4.4 respectively provides gap's cross-sectional area to calculate combustion air velocity and flow rate, where $n_{p,l}$ is the number of particles arranged lengthwise, $n_{p,b}$ is the number of particles arranged breadthwise, L_p is the length of fuel particle and B_p is breadth of fuel particle.

$$H_{cc} = H_f - H_g - r_p \quad 4.1$$

$$H_f = 0.235Q^{2/5} - 1.02D_{i,cc} \quad (4.2)$$

$$\left.\begin{aligned} n_{p,l} &= D_{i,cc}/L_p \\ n_{p,b} &= D_{i,cc}/B_p \\ n_p &= n_{p,l}n_{p,b} \end{aligned}\right\} \quad (4.3)$$

$$n_g = \left(\sum n_{p,l} + 1\right)\left(\sum n_{p,b} + 1\right) \quad (4.4)$$

Determination of air requirement and flame temperature

The fuel is composed of carbon (*C*), hydrogen (*H*), nitrogen (*N*) and oxygen *(O*) with assumption of no sulphur content. It is considered that about 1g of *C* combines with 2.67 g of *O* to form 1mole of CO_2 and 1g of *H* combines with 8g of *O* to form 1 mole of H_2O. It is known that 1 g of O_2 combines with 3.29g of N_2 to form 4.32g of air. Thus theoretical air requirement (a_{th}) and air supplied (a_s) could be determined as in Eq. 4.5.

$$\left.\begin{aligned} a_{th} &= 4.32(2.67C + 8H - O) \\ a_s &= 2\dot{m} \times a_{th}\,(1 + x) \end{aligned}\right\} \quad (4.5)$$

where, m_f is the burn rate and *x* is the excess air percentage. A factor of 2 is multiplied as both the supplied primary and secondary air are of equal quantity. Assuming moisture content of less than 30% in fuel, the flame temperature *(T_f)* could be determined as in Eq. 3.10. Radiation coefficient is considered as 0.30 as fuel particles are assumed to be greater than 30mm [24], as the fuel particles for experimental validation of SHTM are larger than 30mm.

4.3 Steady state heat transfer modeling of multifunctional biomass fuelled stove

A total of 31 different components of thermal energy are identified for assessment of thermal performance of multifunctional biomass fuelled stove which are illustrated in Fig. 4.4 along with their description in Table 4.2. The principles and methodology discussed in Chapter 3 for performance assessment through development of delineated thermal energy models is also used for proposed multifunctional biomass fuelled stove as discussed below with input parameters provided in Appendix F.

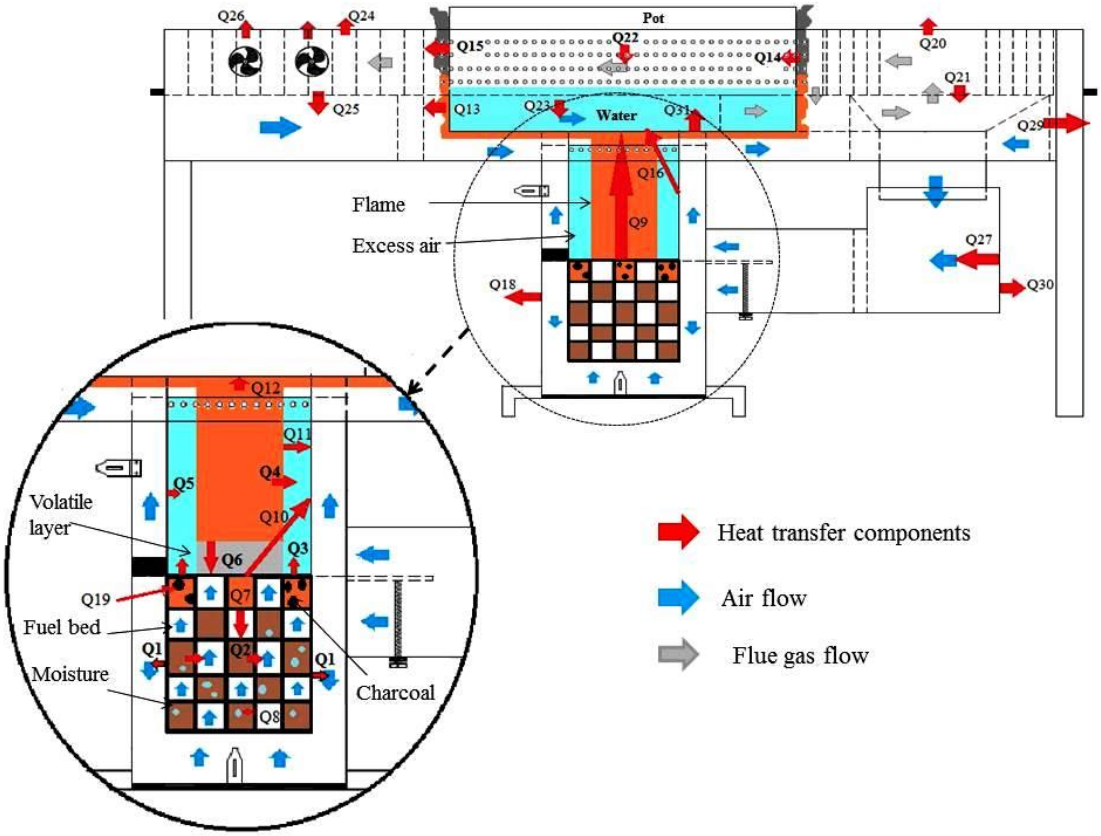

Fig.4.4: Heat transfer components of Multifunctional Biomass Fuelled Stove

Table 4.2: Delineated thermal energy components of a Multifunctional Biomass Fuelled Stove

Sl. No.	Heat transfer component	Sl. No.	Heat transfer component
Q_1	Heat used in heating the incoming air while passing through annular space	Q_{17}	Thermal mass of combustion chamber
Q_2	Heat transferred from fuel bed to primary air while passing through the gaps	Q_{18}	Heat lost from combustion chamber outer wall to ambient
Q_3	Heat transferred by fuel bed to primary air envelope surrounding the inner combustion chamber surface	Q_{19}	Heat left as unburned charcoal
Q_4	Heat lost from flame to excess air	Q_{20}	Heat transferred to pot at top of Spiral Heat Exchanger
Q_5	Heat transferred from combustion chamber inner wall to excess air envelope	Q_{21}	Heat transferred to air at the bottom of Spiral Heat Exchanger
Q_6	Heat transferred from flame to fuel bed	Q_{22}	Reheating of flue gas on passing from Spiral Flow Flue Gas Heat Extractor to Parallel Flow Flue Gas Heat Extractor
Q_7	Heat transferred from fuel bed to bottom layer	Q_{23}	Heat gained by air while passing from Parallel Flow Air pre-heater to Radial flow air pre-heater
Q_8	Heat used for moisture to evaporate	Q_{24}	Heat transferred to water in the pot located above Parallel Flow Flue Gas Heat Extractor

Sl. No.	Heat transfer component	Sl. No.	Heat transfer component
Q_9	Heat transferred from fuel bed to pot bottom	Q_{25}	Heat transferred to air in Parallel Flow Air Pre-heater
Q_{10}	Heat lost from fuel bed to combustion chamber inner wall	Q_{26}	Heat carried by flue gas to ambient
Q_{11}	Heat lost from flame to combustion chamber inner wall	Q_{27}	Pre-heating air while passing through the rectangular duct
Q_{12}	Heat transferred from flame top to pot bottom	Q_{28}	Heat lost as thermal mass of Upper chamber
Q_{13}	Flame to upper chamber	Q_{29}	Heat lost from Upper Chamber outer cover to ambient
Q_{14}	Flue gas to pot outer side surface	Q_{30}	Heat lost from outer wall of rectangular duct
Q_{15}	Flue gas to upper chamber	$Q_{31, BIS}$	Heat received by water in the pot during single pot operation
Q_{16}	Combustion chamber inner wall to pot bottom	$Q_{31, WBT}$	Heat received by water in the pot during multiple pot operation
			BIS Efficiency
			WBT efficiency

4.3.1 Heat received by air while passing through combustion chamber

The combustion air at temperature $T_{a,1}$ is sucked by the in-line fan which is forced through the hot annular chamber over combustion chamber outer cover to receive Q_1 heat and raise its temperature to $T_{a,2}$ as in Eq. 4.6. The convective coefficient of air flowing over the wall as could be determined in Eq. 3.26 [16]. However selection of flow condition depends on the Reynold's number (*Re*) of air flowing at velocity V_{an} over the length of annular space as in Eq. 3.24. The considered density and dynamic viscosity corresponds to air properties at temperature $T_{a,2}$. The value of Q_1 thus obtained provides the combustion chamber outer wall ($T_{cc,o}$) as well as inner wall ($T_{cc,i}$) temperature as in Eq. 4.7 and Eq. 4.8 respectively.

$$Q_1 = (a_s/2) \times c_{p,a} \times (T_{a,2} - T_{a,1}) \quad 4.6$$

$$T_{cc,o} = T_\infty + (Q_1/h_{cc,o}A_{cc,o}) \quad 4.7$$

$$T_{cc,i} = T_{cc,o} + \left((Q_1 \times t_{cc})/(k_{cc} \times A_{cc,o})\right) \quad 4.8$$

where $c_{p,a}$ is air specific heat, $A_{cc,o}$ is outer wall area of combustion chamber, T_∞ is initial temperature of combustion chamber equal to ambient temperature and k_{cc} is thermal conductivity of combustion chamber material.

The primary air at temperature $T_{a,2}$ is then forced through the fuel bed at temperature T_{lb} which is the average of top bed (T_{tb}) and ambient temperature (T_∞). However during operation the top fuel bed's temperature remains in-between the ignition and flame temperature. Therefore for the present study the top bed temperature (T_{tb}) is assumed to

be the average of flame temperature (T_f) calculated as per Eq. 3.10 and ignition temperature (T_{ig}) as mentioned in Table 3.3 as 650 K.

The fuel bed is assumed to contain rectangular ducts of uniform wall thickness distributed uniformly throughout the cross-section of the bed. The walls of the duct are of low thermal conductivity wood and assumed to have constant axial as well as uniform peripheral wall heat flux. This implies version 4 of H2 boundary condition. Thus depending on the boundary condition and aspect ratio (β_g) of the gaps, the Nusselt Number (Nu) could be determined [17] which further provides the heat transfer coefficient ($h_{a,g}$). Whereas hydraulic diameter of the gaps could be determined as the ratio of four times the cross-sectional area w.r.t. perimeter of gaps. Thus during its course through the fuel bed, the air at temperature $T_{a,3}$ which is assumed to reach the ignition temperature T_{ig} i.e. 650K [16] receives Q_2 heat from the inner surface area of the gap walls as in Eq. 3.3.

After taking part in combustion the excess air forms a gap between the flame and combustion chamber inner wall. Thus as there is no contact between the fuel bed and the excess air envelope therefore heat from the fuel bed is transferred through radiation mode. The excess air forms an envelope of thickness equal to the breadth of each gap around the inner wall of the combustion chamber. The radiation heat transferred from the fuel bed at temperature T_{tb} and of cross-sectional area A_{fb} to the primary air at temperature T_x (Q_3) could be determined as in Eq. 3.4. The excess air temperature (T_x) could be determined as the average of the ignition temperature (T_{ig}) and stove's inner wall temperature ($T_{cc,i}$). The view factor (F_{bx}) is considered between the bed with emissivity ε_b and excess air envelope and is determined as in Eq. 4.9 [15].

$$F_{bx} = \frac{1}{2}\left(\frac{H_x}{r_{cc}}\sqrt{4+\frac{H_x^2}{r_{cc}^2}}-\frac{H_x^2}{r_{cc}^2}\right) \qquad 4.9$$

where, H_x is the height of excess air envelope and r_{cc} is the radius of combustion chamber. The excess air envelope height (H_x) is the difference between the stove's height (H_{cc}) and the bed height (H_b). The excess air as it forms an envelope around the flame and the combustion chamber inner wall receives heat from the flame and transfers a part of it to the combustion chamber inner wall continuously. As both the flame and the excess air envelope flows in the same direction and with same velocity,

therefore the relative velocity between them is zero. Thus although both are moving they are static to each other. During the movement the excess air continuously comes in contact with the flame's outer surface. Therefore the excess air at temperature T_x receives heat (Q_4) from the flame at temperature T_f through conduction (due to no relative motion) which could be determined as in Eq. 3.2. The excess air envelope has a thickness of t_x and inner surface area of $A_{i,x}$.

The excess air in a simultaneous process receives heat from the combustion chamber inner wall too while receiving heat from the flame and fuel bed. The excess air at temperature T_x receives heat through both convection (Q_{5a}, Eq. 3.3) from combustion chamber inner wall at temperature $T_{cc,i}$ as well as radiation mode (Q_{5b}, Eq. 3.28) i.e. combined effect of flame as well as combustion chamber. The excess air has an outer surface area of $A_{o,x}$ whose diameter is equal to sum of bed diameter with envelope thickness (t_x) and the height equal to the combustion chamber height.

Depending on the air properties the Reynold's number (*Re*) is calculated as in Eq. 3.24. The flow is considered to be flowing on a plane wall and therefore the coefficient of convective heat transfer ($h_{a,x}$) could be determined using the Eq. 3.26 where the velocity of air is the ratio of mass flow rate of air through combustion chamber (M_a) to the cross-sectional area of the stove (A_{cc}) and the length of travel is the height inside the combustion chamber above the fuel bed.

4.3.2 Heat transferred from the fuel bed

The fuel bed consists of two sections i.e. igniting or top layer and non-combusting or lower fuel bed layer. The top bed layer is assumed to be composed of a single layer of fuel particles and is under continuous mode of ignition. It receives heat both from the flame (Q_6) as well as from the combustion of fixed carbon. The layer of flame is separated from the top of fuel bed by a mixture of volatiles (carbon monoxide, carbon dioxide, hydrogen, methane, ethane, water vapor and oxygen), whose thickness is the ratio of volatiles release rate w.r.t. bed area. The volatiles are assumed to be released at the rate of 70% of burn rate. Heat from the flame to the fuel bed (Q_6) is received through conduction (Q_{6a}) as well as radiation (Q_{6b}) [18] as in Eq. 3.17 and Eq. 3.19 respectively. The view factor between flame bottom and top of fuel bed (F_{fb}) is

determined as in Eq. 3.20 with the considerations that both are of circular cross-section with equal radius (r_{fb}) and separated by a distance (H_{fb}) [19].

In a subsequent process, heat (Q_7) is transferred from top fuel bed at temperature T_{tb} to lower fuel bed at temperature T_{lb} to raise the temperature of fuel particles of lower bed to ignition temperature as in Eq. 3.2. The bed has an area of A_{fb} and thermal conductivity of k_{fb}. However a part of the heat received is lost in evaporating the moisture from fuel (Q_8). The lower fuel bed has an emissivity of ε_{lb}. The heat used in evaporating (Q_8) is product of fuel consumption ($\dot{m}$), moisture content (y_m) and latent heat of vaporization (h_{fg}). Similarly the top burning bed due to an enclosed structure transfers radiation heat to the pot bottom (Q_9) at temperature T_{pb} and combustion chamber inner wall (Q_{10}) at temperature $T_{cc,i}$ as in Eq. 3.4. View factor of fuel bed to combustion chamber inner wall (F_{bcc}) could be calculated as in Eq. 4.9 with similar height and radius equal to combustion chamber's radius. The view factor (F_{bp}) from the fuel bed of radius r_{fb} to the pot bottom with radius r_{pb} with a separation $H_{fb,pb}$ could be determined as in Eq. 4.10 [19].

$$F_{bp} = \frac{1}{2}\left\{Y - \left[Y^2 - 4\left(\frac{r_{pb}}{r_b}\right)^2\right]\right\}^{1/2};\quad Y = 1 + \frac{1+R_2^2}{R_1^2};\quad R_1 = r_{fb}/H_{fb,pb};\quad R_2 = r_{pb}/H_{fb,pb} \tag{4.10}$$

4.3.3 Heat transferred from flame

During cooking the primary pot at temperature T_p remains submerged inside the central hole and is surrounded by an annular ring at temperature T_r which acts like a pot skirt. The annular ring thus forms a gap around the pot through which both flame at temperature T_f as well as flue gas passes. As a result flame transfers heat to the combustion chamber inner wall (Q_{11}) as in Eq. 3.19, pot's outer wall (Q_{12}) and annular ring (Q_{13}). Heat is transferred through both convection and radiation from flame (Q_{12}) with surface area of $A_{f,s}$ to the pot with area of $A_{p,o}$ and annular ring (Q_{13}) of surface area $A_{r,i}$ which could be determined from Eq. 3.3 and Eq. 3.19. The flame has a thickness of t_f, opacity coefficient o, emissivity as considered for 3/4th height (Eq. 3.27) [20] and convective heat transfer coefficient h_f as per Eq. 3.26. The pot, flame and annular ring's surface area could be determined using Eq. 4.11.

$$\left.\begin{aligned} A_{p,o} &= \pi\left(\frac{l_{fp}+\frac{r_p}{2}+\left(\frac{r_r-r_p}{2}\right)}{2}\right)^2 \\ A_{f,s} &= 2\pi\left(\frac{t_f}{2}\right)H_{fb,pb} \\ A_{r,i} &= 2\pi r_r H_r \end{aligned}\right\} \quad 4.11$$

where $H_{fb,pb}$ is the distance between the fuel bed and the pot bottom, r_r is the radius of the annular ring, H_r is the height of annular ring exposed to flame, l_{fp} is the flow path length over pot's outer surface, r_p is the pot radius and r_{ar} is the annular ring radius.

The view factor between flame and pot F_{fp} is calculated as in Eq. 4.10 by replacing r_{fb}, r_{pb} and $H_{fb,pb}$ by pot radius r_p, flame travel length over pot surface and $H_{ft,pb}$ (distance between the flame top and the pot bottom) respectively. The flame travel length over the pot outer wall could be determined as the difference between calculated flame height as in Eq. 4.2 and the cumulative sum of pot stand height, pot radius and half the combustion chamber height. The annular ring's height is equal to pot's height which is determined from the power delivery vs pot dimension relationship according to BIS [21]. The height of annular ring exposure to flame (H_{fr}) could be determined as the difference between flame height and the half the sum of combustion chamber's height and pot's diameter. The rest of the annular ring's height ($L_{fg,r}$) pertaining to an area of $A_{fg,r}$ is exposed to the flue gas at temperature T_{fg} i.e. average of ignition (T_{ig}) and flame temperature (T_f).

Similarly as the flue gas passes, it transfers Q_{14} and Q_{15} heat to both the pot outer wall at temperature T_{pb} and annular ring at temperature T_r respectively which could be determined as in Eq. 3.3. Flow condition is considered to be as fluid passing over plain wall to determine convective heat transfer coefficient ($h_{fg,r}$) as in Eq. 3.26. Flow type of flue gas based on Reynolds number is determined using Eq. 3.24 considering flue gas density and dynamic viscosity corresponding to the flue gas temperature (T_{fg}) flowing with velocity (V_{fg}) over a length of ($L_{fg,r}$). The flue gas velocity is determined from both the rates of air supplied and volatiles released with respect to cross-sectional area of combustion chamber. The flue gas is then sucked through the perforations on the annular ring to the flue gas heat extractors using induced draft fans. Heat transfer to various sections of heat extractors and air pre-heaters are discussed in Section 4.4.6.

4.3.4 Heat transfer from combustion chamber

The combustion chamber is divided into two sections i.e. inner combustion chamber and outer cover. During combustion the inner wall of the combustion chamber having area $A_{cc,i}$ maintains a higher temperature ($T_{cc,i}$) with respect to pot bottom (T_{pb}) with emissivity ε_{cc}. Thus a part of the heat (Q_{16}) is radiated to the pot bottom from the combustion chamber inner wall as in Eq. 3.4 with view factor $F_{cc,p}$, combustion chamber emissivity of ε_{cc}.

As already discussed the inner combustion chamber of the present design forms an integral part with the outer cover to form the stove system. Thus a part of the heat received by the combustion chamber is transferred to the thermal mass of the outer cover (Q_{17}) during the entire period of operation as in Eq. 4.12. This could be determined as the rise in outer cover's initial temperature ($T_{i,s}$) to an elevated temperature ($T_{f,s}$) at which the steady state is maintained.

$$Q_{17} = m_s c_{p,s}\left(T_{f,s} - T_{i,s}\right) \tag{4.12}$$

where m_s is the mass of the stove and $c_{p,s}$ is the specific heat of the stove. As a result the outer cover of area A_{oc} maintaining a higher temperature (T_{oc}) starts losing heat (Q_{18}) through both convection (Q_{18a}) and radiation mode (Q_{18b}) to the ambient at temperature (T_{∞}) as in Eq. 3.3 and Eq. 3.4. The stove's outer cover has an emissivity of ε_{oc} and air flows with convective heat transfer coefficient $h_{a,oc}$ as Eq. 3.26 depending on the Reynold's number. The ambient air is assumed to be flowing at velocity (V_a).

Thus the amount of heat utilized (Q_U) and total heat lost (Q_L) could be determined as in Eq. 4.13, as a result heat lost as charcoal (Q_{19}) could be determined.

$$Q_L = Q_i - Q_U = m_f(CV)_f - (Q_9 + Q_{12} + Q_{14} + Q_{16}) = Q_1 + Q_2 + Q_3 + Q_4 + Q_5 + Q_6 + Q_7 + Q_8 + Q_9 + Q_{10} + Q_{11} + Q_{17} + Q_{18} + Q_{19} \tag{4.13}$$

4.3.5 Flue gas heat extraction and air pre-heating

Heat exchange in Spiral Flow Flue Gas Heat Extractor

The flue gas still retains Q_{fg} heat in it while being sucked inside the upper chamber as could be determined in Eq. 4.14. The air flows in counter flow direction while passing

through the parallel (PAH) and radial flow air pre-heaters (RAH) w.r.t. flue gas which passes through spiral (SHE) and parallel flow heat extractors (PHE) respectively. Both the flue gas heat extractors and air pre-heaters are of same height (H_{HE}) which is half the pot's height. The flue gas thus while passing through the SHE transfers Q_{20} and Q_{21} heat to the top plate and RAH beneath it respectively as in Eq. 4.15 and Eq. 4.16 respectively. Both the flue gas as well as air passes through connector channels while intra-changing between heat exchangers receiving Q_{22} and Q_{23} heat respectively. Before exiting i.e. while passing through PHE, the flue gas transfers Q_{24} and Q_{25} amount of heat to the top conducting plate and bottom PAH respectively.

$$Q_{fg} = (2a_s + \dot{m})\left[60.41T_f - (3.45 \times 10^{-3})T_f^2 + (1.98 \times 10^{-7})T_f^3 - (2.35 \times 10^{-9})T_f^4 - 37443.76\right] \quad 4.14$$

$$Q_{20} = U_{SHE} A_{SHE} (T_{fg} - T_w) \quad 4.15$$

$$Q_{21} = m_{a,RAH} c_{p,a,RAH} (T_{a,1} - T_{a,2}) \quad 4.16$$

where, a_s is air supplied, $\dot{m}$ is fuel burn rate, T_f is flame temperature, A_{SHE} is the SHE top area, T_{fg} is the flue gas temperature and T_w is the water at ambient temperature whereas $m_{a,RAH}$, $c_{p,a,\ RAH}$, $T_{a,1}$ and $T_{a,2}$ are mass flow rate, specific heat, outlet temperature and inlet temperature of air through RAH . The designed SHE has a plate length of L_p, outer diameter of D_{SHE} as in Eq. 4.17 and number of turns (n_t) as in Eq. 4.18 [22].

$$D_{SHE} = \sqrt{1.28 L_p (L_s + 2t_p) + D_{i,SHE}^2} \quad 4.17$$

$$n_t = (1/L_s)\left((2D_{SHE}/\pi) - D_{i,SHE}\right) + 1 \quad 4.18$$

where L_s is plate spacing, t_p is plate thickness and $D_{i,SHE}$ is inner diameter. The overall heat transfer coefficient of the flue gas passing through the spiral flow channel (U_{SHE}) could be determined as in Eq. 4.19.

$$U_{SHE} = 1/((1/h_{SHE}) + (t_p/k_p) + (t_{pb}/k_{pb})) \quad 4.19$$

where t_p and t_{pb} are the thickness of top plate and pot respectively, whereas k_p and k_{pb} are thermal conductivity top plate and pot respectively. The convective heat transfer

coefficient of flue gas inside SHE (h_{SHE}) [23] is determined as in Eq. 4.20 which depends on Reynold's number (Re_{SHE}) and Critical Reynold's number ($Re_{c,SHE}$, Eq. 4.21).

$$h_{SHE} = \begin{cases} \left(1 + 3.54\frac{D_{h,SHE}}{D_{SHE}}\right) 0.023 c_{p,fg,SHE} V_{fg,SHE} Re_{SHE}^{-0.2} Pr_{SHE}^{2/3}, & (For\ Re_{SHE} > Re_{c,SHE}) \\ 1.86 c_{p,fg,SHE} V_{fg,SHE} Re_{SHE}^{-2/3} Pr_{SHE}^{-2/3} \left(\frac{L_p}{D_{h,SHE}}\right)^{-1/3} \left(\frac{\mu_{w,1}}{\mu_{b,1}}\right)^{-0.14}, & (For\ 100 < Re_{SHE} < Re_{c,SHE}) \end{cases} \quad 4.20$$

$$Re_{c,SHE} = 20000\left(D_{h,SHE}/D_{SHE}\right)^{0.32} \quad 4.21$$

where, $D_{h,SHE}$, $c_{p,FG,SHE}$, $V_{FG,SHE}$, Pr_{SHE} , $\mu_{w,1}$ and $\mu_{b,1}$ are hydraulic diameter, specific heat, velocity, Prandtl Number, viscosity at SHE wall temperature and bulk viscosity of flue gas in SHE respectively. Therefore total useful heat extracted from flue gas on passing through SHE is the sum of Q_{20} and Q_{21}, while the flue gas temperature drops to exit temperature of $T_{fg,1}$ and enters the flue gas connector channel.

Heat exchange in connector channels

The rectangular flue gas connector channel has one of its outer faces heated by hot flame and incoming hot flue gas, which reheats the flue gas by Q_{22} heat while passing through it to PHE as in Eq. 4.22.

$$Q_{22} = h_{fg,co} A_{fg,co} (T_{w,fg,co} - T_{fg,i}) \quad 4.22$$

where $A_{fg,co}$ is the connector channel side wall area, $T_{w,fg,co}$ is the side wall temperature of the connector channel and $T_{fg,i}$ is the flue gas temperature at inlet of flue gas connector channel. The flow condition of flue gas follows version 1L of H1 boundary condition and thus the Nusselt number ($Nu_{fg,co}$) could be obtained directly from literature [17]. The heat transfer coefficient ($h_{fg,co}$) could therefore be determined as the ratio between $Nu_{fg,co} k_{fg,co}$ and $D_{h,co}$, where $k_{fg,co}$ is the thermal conductivity of the flue gas and $D_{h,co}$ is the hydraulic diameter of the connector channel.

Similarly prior to the entry inside RAH the air receives Q_{23} amount of heat while passing through the connector channel as in Eq. 4.23. But in this case three of the sides

of the connector channel is heated by hot flue gas and flame thus following version 3L of H1 boundary condition [17].

Thus, the value of Nusselt number ($Nu_{a,co}$) could be determined [17] which further provides the heat transfer coefficient ($h_{a,co}$) of air flowing through it.

$$Q_{23} = h_{a,co} A_{a,co} (T_{w,a,co} - T_{a,i}) \quad 4.23$$

where $A_{a,co}$, $T_{w,a,co}$ and $T_{a,i}$ are wall area, temperature of the wall and inlet air temperature at of connector channel.

Heat exchange in Parallel Flow Flue Gas Heat Extractor

The reheated flue gas then enters the parallel flow flue gas heat extractor (PHE). Heat from the flue gas is further transferred to the top conducting plate (Q_{24}) and air flowing beneath through the parallel flow air pre-heater (PAH) in cross-flow direction (Q_{25}). Both the PHE and PAH consists of arrays whose flow conditions are assumed to be [23]:

a. Steady state condition with fully developed flow throughout each channel

b. Constant flow and boundary properties with ideal gas behavior

c. Negligible kinetic and potential energy changes with negligible conduction resistance for end plates

The number of arrays that could be adjusted in both PHE and PAH depends on number of fins (N) which could be determined as the ratio of heat exchanger width (W) and pitch (p) i.e. W/p. Therefore the total surface area of each array (A_t), overall efficiency of heat exchanger (η_o) and fin efficiency (η_f) could be determined as in Eq. 4.24 and Eq. 4.25 respectively [19].

$$A_t = NA_f + A_b = 2N(L/2)B + (W - Nt)B \quad 4.24$$

$$\eta_o = 1 - ((NA_f)/A_t)(1 - \eta_f);\ \eta_f = tanh\, m\left(\frac{L}{2}\right) / \left(m\left(\frac{L}{2}\right)\right);$$

$$m = (2h(t + B)/k(t + B))^{1/2} \quad 4.25$$

where A_f is the fin area, A_b is the base area, L is the fin height, B is the length of PHE or PAH and t is the fin thickness. Each channel has an aspect ratio of $L/(p-t)$ which could be used to determine Nusselt Number directly from literature for laminar flow. However for turbulent flow i.e. $0.5<Pr<2000$ and $3000<Re_D<5\times10^6$, Nusselt Number could be determined as in Eq. 4.26 [19]. Thus the convective heat transfer coefficient (h), hydraulic diameter (D_h) and Reynolds' Number (Re) of the fluid flowing through both PAH and PHE could be determined as in Eq. 4.27.

$$Nu = ((f/8)(Re-1000)Pr)\Big/\left(1+12.7\left(\frac{f}{8}\right)^{\frac{1}{2}}\left(Pr^{\frac{2}{3}}-1\right)\right) \quad 4.26$$

$$h = \frac{Nu\ k}{D_h};\ Re = \frac{M_f D_h}{A_c \mu};\ D_h = (4L(p-t))/(2(L+p-t) \quad 4.27$$

where f is the friction factor, M_f is the fluid flow rate and can be either flue gas or air, A_c is the cross-sectional area and μ is the dynamic viscosity of the fluid. Each array has a thermal resistance of R_t which could be determined as $(\eta_o h A_t)^{-1}$. As a result the surface temperature (T_s) as well as log mean temperature difference (θ_1) could be determined as in Eq. 4.28.

$$\theta_1 = \big((T_i - T_s) - (T_o - T_s)\big)/(\ln[(T_i - T_s)/(T_o - T_s)])\,;\ T_s = \frac{T_i e^{\left(-1/(m_f c_p R)\right)} - T_o}{e^{\left(-1/(m_f c_p R)\right)} - 1} \quad 4.28$$

where R is $r/2$, T_i is the fluid inlet temperature and T_o is the fluid outlet temperature. The total heat extracted ($Q_{fg,1}$) from the flue gas could be determined as $2hA_t\eta_o\theta_1$ and thus the heat flux ($\dot{Q}$) of the PHE could be determined as in Eq. 4.29.

$$\dot{Q} = Q_{fg,1}/\{2[B\times W + W(L+2t) + B(L+2t)] + 2(N-2)L\times B\} \quad 4.29$$

Thus heat transferred from PHE to top conducting plate (Q_{24}) could be determined as $\dot{Q}BW$ which further provides us the log mean temperature difference of PAH (θ_2) as in Eq. 4.30. Thus the overall heat transfer efficiency ($\eta_{o,PAH}$) and fin efficiency ($\eta_{f,PAH}$) for PAH could also be determined using Eq. 4.25. Similarly the heat transferred to air on passing through PAH (Q_{25}) and heat carried by flue gas (Q_{26}) could be determined as in Eq. 4.31 and Eq. 4.32 respectively.

$$\theta_2 = Q_{25}/2hA_t\eta_{o,PAH} \quad 4.30$$

$$Q_{25} = 2h_aA_{t,PAH}\eta_{o,PAH}\theta_2 \quad 4.31$$

$$Q_{26} = (2a_s + m_f)\left[60.41T_{fg,o} - (3.45 \times 10^{-3})T_{fg,o}^2 + (1.98 \times 10^{-7})T_{fg,o}^3 - (2.35 \times 10^{-9})T_{fg,o}^4 - 37443.76\right] \quad 4.32$$

where h_a is the convective heat transfer coefficient of air, $A_{t,PAH}$ is the total heat transfer area of the parallel flow air pre-heater, a_s is the air supplied and $T_{fg,o}$ is the flue gas outlet temperature. The pre-heated air after passing through the RAH enters a rectangular duct with hydraulic diameter ($D_{h,RD}$) of $2LB/(L+B)$, where L is the length and B is the breadth of the rectangular duct. The air flow through the duct follows the version 4 of H1 boundary condition [17], thus depending on the aspect ratio (B/L) the Nu_{RD} could be determined directly as well as convective coefficient (h_{RD}) of air as in Eq. 4.27. Therefore the heat received by air while passing through the rectangular duct (Q_{27}) could be determined as in Eq. 4.33.

$$Q_{27} = h_{RD}A_{RD}(T_{w,RD} - T_{a,RD}) \quad 4.33$$

where A_{RD} is the surface area of the rectangular duct, $T_{w,RD}$ is the temperature of rectangular duct and $T_{a,RD}$ is the temperature of air flowing through the rectangular duct. During the process of heat extraction from flue gas losses are incurred in thermal mass of upper chamber (Q_{28}), from outer wall of upper chamber (Q_{29}) and from outer wall of rectangular duct (Q_{30}) as in Eq. 4.34, Eq. 4.35 and Eq. 4.36 respectively. The outer cover due to its higher temperature losses heat through both convective ($Q_{29,a}$) as well as radiation ($Q_{29,b}$) mode respectively to the ambient.

$$Q_{28} = m_{UC}c_{p,UC}(T_{UC} - T_\infty) \quad 4.34$$

$$\left.\begin{aligned} Q_{29,a} &= h_{a,UC}A_{UC}(T_{UC} - T_\infty) \\ Q_{29,b} &= \varepsilon_{UC}\sigma A_{UC}(T_{UC}^4 - T_\infty^4) \end{aligned}\right\} Q_{29} = Q_{29a} + Q_{29b} \quad 4.35$$

$$Q_{30} = h_{a,R}A_R(T_R - T_\infty) + \varepsilon_{RD}\sigma A_{RD}(T_{RD}^4 - T_\infty^4) \quad 4.36$$

where m_{UC}, $c_{p,UC}$, T_{UC}, $h_{a,UC}$, A_{UC}, ε_{UC}, σ, $h_{a,R}$, A_{RD}, T_{RD} and ε_{RD} are the upper chamber's mass, upper chamber's specific heat, upper chamber's temperature, convective coefficient of air over upper chamber, exposed area of upper chamber to ambient, upper

chamber emissivity, Boltzmann Constant, outer area of rectangular duct, outer surface wall temperature and emissivity of rectangular duct respectively. The value of $h_{a,UC}$ and $h_{a,RD}$ could be determined from Eq. 3.26.

Different components of heat in specific heat transfer network are modeled in terms of range of parameters. The multifunctional biomass fuelled stove designed for current features can be operated under 2 modes *viz.* (i) single pot operation and (ii) multiple pot operation. Accordingly assessment of performance of newly designed stove has been done for both the options. The single pot operation which is in line with standard test protocols of BIS required 19 number of component models developed in these sections. Similarly performance assessment for multiple pot operation required 31 components which are as per standard protocol of WBT. The details of performance assessment are discussed below.

4.3.6 Performance of the stove

Pot energy balance

In the above SHTM the heat received for single pot application ($Q_{31,BIS}$) and multiple pots ($Q_{31,WBT}$) varies and therefore could be determined as in Eq. 4.37 and Eq. 4.38.

$$Q_{31,BIS} = Q_9 + Q_{12} + Q_{14} + Q_{16} \quad 4.37$$

$$Q_{31,WBT} = Q_9 + Q_{12} + Q_{14} + Q_{16} + Q_{20} + Q_{24} \quad 4.38$$

Stove's efficiency

Thus the efficiency of stove varies for both single and multiple pot applications. The single pot cooking resembles the BIS approved cook stove test whereas multiple pot cooking resembles WBT procedure. Therefore the efficiencies according to BIS (η_{BIS}) and WBT (η_{WBT}) could be determined as in Eq. 4.39 and Eq. 4.40 respectively.

$$\eta_{BIS} = \frac{Q_{31,BIS}}{\dot{m} \times CV_f} \quad 4.39$$

$$\eta_{WBT} = \frac{Q_{31,WBT}}{\dot{m} \times CV_f} \quad 4.40$$

where $\dot{m}$ and CV_f are the burn rate of fuel and calorific value of fuel respectively.

Time to boil

The time to boil for the given stove is the time taken to boil the primary pot which is similar for the both the testing procedures i.e. BIS and WBT, as both test procedures considers the time taken to boil primary pot. Therefore the time to boil is determined as in Eq. 4.41.

$$Time\ to\ boil = \frac{(m_{w,evap} \times c_{p,w} \times (T_b - T_i))}{Q_{31,BIS}} \quad 4.41$$

where, $m_{w,evap}$, $c_{p,water}$, T_b and T_i are the mass of water evaporated, specific heat of water, boiling water temperature and initial water temperature respectively. The mass of water boiled could be determined as in Eq. 4.42.

$$m_{w,evap} = Q_{evap}/h_{fg} \quad 4.42$$

where Q_{evap} is the heat utilized for evaporation and is determined as in Eq. 4.43 and h_{fg} is the latent heat of vaporization.

$$Q_{evap} = Q_{31,BIS} - Q_b \quad 4.43$$

where Q_b is the heat required to boil and is determined as in Eq. 4.44.

$$Q_b = A_{p,i} Q_B^{"} \quad 4.44$$

where $A_{p,i}$ is the area of contact between the water and pot, and heat flux ($Q_B^{"}$) is determined from Eq. 3.34 [19, 23-24]. The water is considered to have an excess temperature within nucleate pool boiling condition i.e. between 5°C and 30°C [24].

4.3.7 Experimental test methodology

The designed stove is further manufactured and tested under controlled laboratory conditions. As the designed stove has the features of both single and multiple pot stoves, therefore its performance evaluation will be incomplete if tested for single pot tests such as BIS [24]. Thus in addition to BIS, the designed stove is also tested using WBT [25] in order to measure its multiple pot cooking potential. The obtained results are further compared with test results of other available and reported solid fuelled stoves.

The designed stove is a forced draft stove and provides optional usage of using the upper chamber along with the stove. Preliminary BIS tests are conducted in order to obtain the optimized flow rate of air for highest efficiency using upper chamber as attachment. Further usefulness of the upper chamber in terms of efficiency is justified through comparative analysis with respect to BIS tests without upper chamber. However WBT tests are conducted using upper chamber as attachment for the designed stove.

BIS Test procedure

The BIS test procedure initially involves determination of size of the cook stove and its power output for selection of amount of water and pot size [24]. This test is performed by operating the stove without any load to determine the fuel consumption rate (kg/s), which further provides the power output (kW). Depending on the power output the size and mass (W_p) of Aluminium vessel as well as the amount of water (W_w) for the test is selected. In the present study continuous feeding of fuel having calorific value NCV_f, is performed while placing the vessel containing water with lid above it. Two such vessels are used for the test and fuel is arranged in order to continue the test for one hour. The fuel lot (W_f) is divided into 10 equal quantities. Initially the stove is filled with the first lot and pot containing water at ambient temperature (T_∞) and lid is placed on the stove. The top lid contains a hole to insert the thermocouple for temperature measurement. The fuel is then lit and stop watch is set for one hour. The test is continued with continuous feeding in an interval of 6 minutes. The pot is replaced with the second pot with lid containing fresh water as soon as the first pot reaches 95°C (T_2). The cycle is repeated for one hour. At the end of test duration i.e. one hour, the number of pots replaced (x) and the final temperature of the water (T_f) in the pot is noted. Thus the efficiency (η) of the stove could be determined as in Eq. 4.45 [24].

$$\eta = \frac{[(x-1)\times(W_p\times c_v+W_w\times c_w)\times(T_2-T_\infty)]+\left[(W_p\times c_v+W_w\times c_w)\times\left(T_f-T_\infty\right)\right]}{\left(W_f\times NCV_f\right)+(W_k\times NCV_k)}\times 100 \qquad 4.45$$

where c_v, c_w, W_k and NCV_k are the specific heat of vessel, specific heat of water, weight of additional kerosene and calorific value of kerosene initially required to ignite the fuel respectively.

Water Boiling Test (WBT) procedure

The WBT procedure involves three stages of testing i.e. high power cold start, high power hot start and low power simmering test [25]. In the present study three pots are used for each test i.e. one primary pot placed at the middle whereas another secondary and tertiary pots placed at both the sides of the primary pot. During each test the primary pot is filled with 5 liters of water whereas both the secondary and tertiary pots are filled with 1.5 liters water each. The tests are conducted without using lid. During cold start the stove at room temperature is ignited with fuel with measured calorific value and quantity. The test is stopped as soon as the water in primary pot gets boiled and the time taken to boil the primary water, fuel consumed, water evaporated from all pots and charcoal left are measured. The hot water is then replaced with fresh water while the stove is still hot and fresh fuel is fed for the hot start phase. The test is repeated similar to cold start and measurements are repeated. However at the end of hot start test phase both hot water and charcoal are not replaced. The hot start phase is immediately followed by the simmering phase which is performed for 45 minutes. Fuel is fed in such a way that the temperature of water in primary pot maintains a temperature between local boiling point and not less than 6°C from the local boiling point. Unlike the previous two phases only changes in water weight, fuel consumed and charcoal left are measured. Both the cold and hot start provides the thermal efficiency, specific fuel consumption, temperature corrected specific consumption as well as specific energy consumption and firepower. Additional information of turn down ratio could be determined using the simmering test data.

Measuring instruments

Both the above test procedures involve measurement of parameters related to temperatures, weight and flow rate. These measured parameters are further used to determine the performance parameters. The instruments which are used in the present study are listed in Table 4.3.

Table 4.3: List of instruments

Sl. No.	Instrument	Parameters measured
1.	Thermocouple	• Water temperature • Surface temperatures
2.	Weighing balance	• Water weight • Fuel weight

Sl. No.	Instrument	Parameters measured
3.	Anemometer	• Air flow rate • Flue gas flow rate

4.3.8 Error and uncertainty analysis

Measurements during experiments may involve errors caused due to human error, instrumental resolution, calibration, environmental factors, zero offset, physical variations, parallax, instrument drift, lag time and hysteresis. Similarly uncertainty analysis is the measurement of uncertainty amongst the measured values obtained through experimentation.

The uncertainty amongst the experimental results may be reduced considering average values. However its accuracy remains doubtful. Therefore determination of standard deviation acts as one of the common method to check the spread of the data obtained. The standard deviation (*S*) of a data set is determined as in Eq. 4.46 [26].

$$S = \sqrt{\frac{\sum_{i=1}^{N} \delta x_i^2}{(N-1)}} \tag{4.46}$$

where *N* is the number of experimental data and *x* is the data value. However the uncertainty associated with the average value should be smaller with increase in number of measurements. Thus the standard deviation associated with the average is known as standard error (σ) and could be determined as in Eq. 4.47 [26].

$$\sigma = \frac{S}{\sqrt{N}} \tag{4.47}$$

Another factor determining the precision of a measured set of values is the fractional uncertainty which could be determined as in Eq. 4.48 [26].

$$Fractional\ uncertainity = \frac{Uncertainity}{Average} \tag{4.48}$$

where uncertainty is the standard error (σ) as mentioned in Eq. 4.47 and average is the average of the measured values.

4.4 Results and discussions

4.4.1 Steady state heat transfer analysis

The developed SHTM for the multifunctional biomass fuelled stove is further used to analyze the various heat transfer components inside the stove. The SHTM is applied to 4.5 kW output multifunctional biomass fuelled stove. The fuel bed of $5.5\times6.22\times10^{-4}$ m^2 consist gaps having average cross-section, perimeter and aspect ratio of 4.01×10^{-4} m^2, 0.12 m and 5.91 respectively. During operation bed at temperature 446.53 K releases volatiles at the rate of 1.72×10^{-4} kg/s.

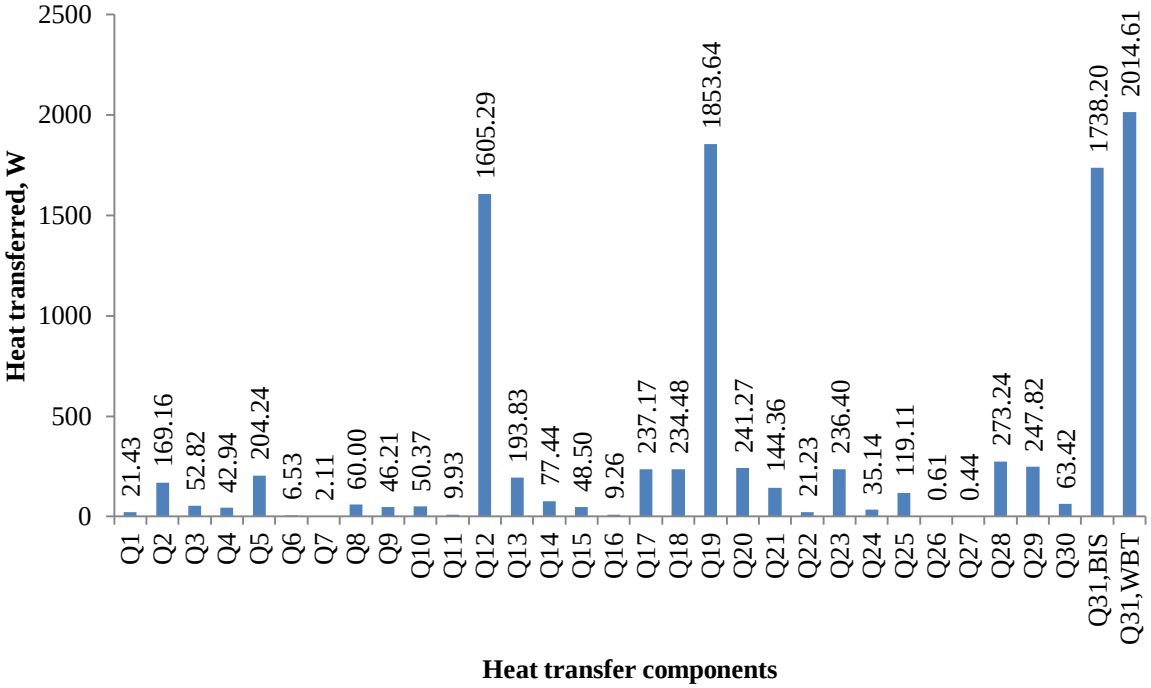

Fig.4.5: Steady state heat transfer analysis of Multifunctional biomass fuelled stove

The inline fan during operation supplies air of 1.95×10^{-3} m^3/s at 678.65 K as both primary and secondary air as measured during experiments. As a result air receives 21.43 W (Q_1) as in Fig. 4.5 with convective coefficient of 7 W/m^2K and raises its temperature to 455.25 K. The air further passes through the gaps at 868.90 K of fuel bed having aspect ratio of 6 and hydraulic diameter of 1.28×10^{-2} m at a flow rate of 6.87×10^{-1} m/s. During its flow the air receives 169.16 W (Q_2) heat as in Fig. 4.5 with Nusselt number of 5.62 and convective heat transfer coefficient of 16.15 W/m^2K. The air mass flux i.e. 4.41×10^{-1} kg/m^2s thus obtained results in flame temperature and height of 1087.81 K and 0.34 m.

The excess air after flowing through the gaps forms an envelope at 664.35 K filling the gap between flame and combustion chamber and shares surface areas of 1.94×10^{-2} m^2 and 5.27×10^{-2} m^2 respectively. The air flows at 3.91×10^{-1} m/s over the flame having convective coefficient of 5.33 W/m^2K. The envelope thus formed receives heat of 52.82 W (Q_3), 42.94 W (Q_4) and 204.24 W (Q_5) as in Fig. 4.5. It forms a view factor of 0.89 as in Table G.1 of Appendix G with the fuel bed. The flame and combustion chamber are considered to have emissivity of 0.82 and 0.2 respectively.

The flame on the other hand transfers heat of 4.90 W (Q_{6a}) and 1.63 W (Q_{6b}) to the fuel bed through both conduction and radiation respectively. The base of flame has an emissivity of 0.18 with opacity coefficient of 0.73 and has a view factor of 0.73 with fuel bed as in Table G.1 of Appendix G. While the lower fuel bed receives additional heat of 2.11 W (Q_7) from the top fuel bed. However lower bed absorbs heat of 60 W (Q_8) to evaporate 10% moisture in fuel.

In a subsequent process heat of 46.21 W (Q_9) is received by the pot bottom from the fuel bed having emissivity of 0.82 and view factor of 0.53. Similarly the fuel bed and flame with emissivity of 0.14, transfers radiation heat of 50.37 W (Q_{10}) and 9.93 W (Q_{11}) to the combustion chamber. The fuel bed and the flame maintain view factors of 0.89 and 0.99 with the combustion chamber as in Table G.1 of Appendix G. As the flame exits the combustion chamber it flows at 7.51×10^{-1} m/s over pot as well as annular ring's surfaces with 1.16×10^{-1} m^2 at 377.15 K and 1.11×10^{-1} m^2 at 678.69 K respectively. The flame thus radiates heat of 781.79 W (Q_{12a}) and 25.62 W (Q_{13a}) to the pot as well as annular ring respectively and 823.49 W (Q_{12b}) and 168.22 W (Q_{13b}) through convection respectively. View factors of 1 and 0.69 is maintained by the flame with the pt and annular ring respectively as in Table G.1 of Appendix G with convective coefficient of 6.91 W/m^2K and 3.70 W/m^2K respectively. The flame on exposure to colder surfaces forms the flue gas and therefore transfers convective heat of 77.44 W (Q_{14}) and 48.50 W (Q_{15}) to the top portions of pot and annular ring of 2.20×10^{-2} m^2 and 4.28×10^{-2} m^2 respectively with convective coefficient of 7.17 W/m^2K and 5.96 W/m^2K respectively.

The combustion chamber on the other hand radiates heat to the pot bottom of 9.26 W (Q_{16}), absorbs heat of 237.17 W (Q_{17}) and losses radiation heat of 72.05 W (Q_{18a}) as well as convection heat of 162.44 W (Q_{18b}) to the ambient. The pot and combustion

chamber has a view factor of 0.15. Therefore at the end of SHTM for single pot application a total of 1738.20 W (Q_{30}) is utilized and 908.16 W is lost without using the upper chamber. Thus the model predicts that the stove will operate at an efficiency of 38.63% and can boil 6.10 kg water in 18.49 minutes considering single pot operation which resembles BIS test procedure. Energy balance shows that the 1853.64 W (Q_{18}) heat is trapped as charcoal produced at 6.18×10^{-5} kg/s.

The hot flue gas at 868.90 K upon exiting the combustion chamber enters the SHE channel having hydraulic diameter of 3.11×10^{-2} m and at 583.53 K. The hot flue gas entering the SHE flows at a rate of 6.24×10^{-3} m^3/s and transfers 241.27 W (Q_{19}) to the water in the secondary pot with overall heat transfer coefficient of 18.77 W/m^2K. Similarly an amount of 144.35 W (Q_{20}) is received by the air flowing through RAH at 4.77×10^{-3} kg/s and gets preheated to 446.35 K. The flue gas exiting the SHE is again reheated by 21.22 W (Q_{21}) with convective coefficient of 7.80 W/m^2K while passing through the connector channel with aspect ratio of 0.29. The walls of the connector channel are maintained at 868.90 K. In a similar way heat of 236.40 W (Q_{22}) is transferred to the air passing through connector channel flowing beneath. The air through the connector channel receives heat with convective coefficient of 4.47 W/m^2K at overall efficiency of 56% and LMTD of 531.67 K.

The flue gas at last passes through the PHE transferring 35.14 W (Q_{23}) to the water placed in the pot located above PHE at convective coefficient of 10.52 W/m^2K. The LMTD of the flue gas flowing through PHE is 106.98 K with overall PHE efficiency of 22%. Simultaneously about 119.11 W (Q_{24}) is transferred to the air passing through PAH from the flue gas in PHE. The air flows with LMTD of 301.86 K and overall efficiency of 71%. The flue gas after transferring heat to both the water located above PHE and air flowing through PAH finally exits the upper chamber retaining 0.61 W (Q_{25}) within it. The preheated air thus exiting through the RAH outlet is forced to pass through the rectangular duct with aspect ratio of 0.29 at 868.90K. The air flowing at 4.22×10^{-3} kg/s is therefore again preheated by 277.43 W (Q_{26}) with convective coefficient of 8.50 W/m^2K. Subsequently an amount of 273.24 W (Q_{27}), 247.82 W (Q_{28}) and 63.42 W (Q_{29}) heat are lost to the thermal mass of the upper chamber (Q_{27}) and from the skin of both upper chamber (Q_{28}) and rectangular duct (Q_{29}) respectively.

The SHTM therefore predicts that in multifunctional biomass fuelled stove an amount of 1738.20 W ($Q_{31,BIS}$) is utilized during single pot operation (BIS) whereas it rose to utilization of 2014.61 W ($Q_{31,WBT}$) during multiple pot operation (WBT). Thus according to SHTM the multifunctional biomass fuelled stove operates at 38.63% during single pot operation (BIS) whereas the efficiency rose to 44.77% during multiple pot operation (WBT) as in Fig. 4.6. However in order to validate the SHTM results earlier reported results are needed. Therefore due to absence of any reported data a prototype is to be manufactured and tested for its performance. A comparative analysis between the SHTM results and the experimental results will thus validate the SHTM results.

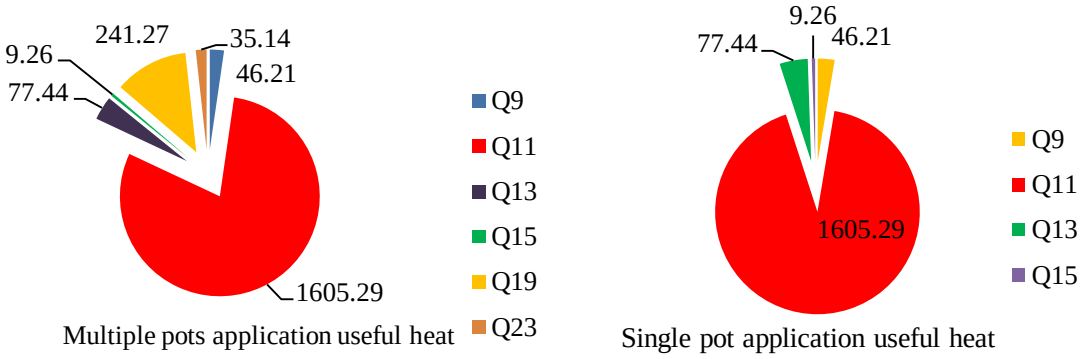

Fig.4.6: Comparative analysis of useful heat contribution during multiple pots and single pot test using SHTM for 4.5 kW Multifunctional biomass fuelled stove

4.4.2 Experimental performance test results of the developed stove

(a) (b)

(c) (d)

Fig.4.7: Prototype of Multifunctional biomass fuelled stove

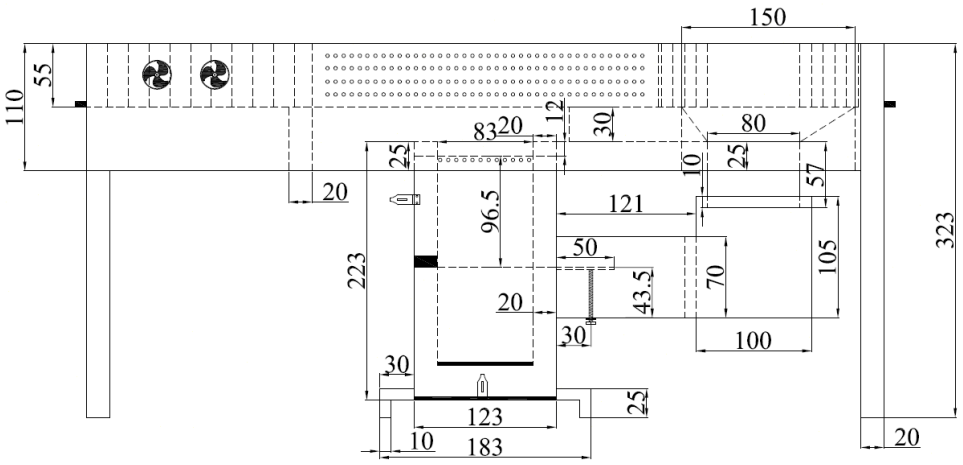

(a)

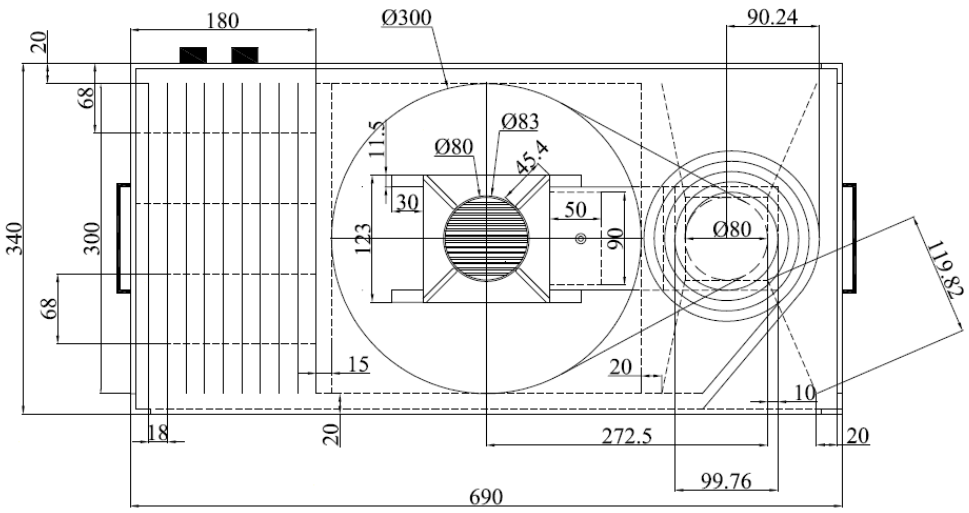

(b)

Fig. 4.8: Dimensions of Multifunctional biomass fuelled stove (a) front view (b) top view (All dimensions are in mm)

The manufactured multifunctional biomass fuelled stove as shown in Fig. 4.7 and Fig. 4.8 is further tested for its efficiency using two recognized and well established test procedures i.e. BIS approved cook stove test [24] and standard WBT [25]. The obtained results of which are discussed below in the subsequent sections. Uncertainties and errors pertaining to the obtained results are also discussed as an integrated part of the test results for each category of test procedures. Further the performance of the manufactured multifunctional biomass fuelled stove is compared with other available stoves. During the tests fuel particles having moisture content of 5% ±1% and 10% ± 1% are used for BIS and WBT tests respectively.

4.4.2.1 Bureau of Indian Standards test results

The multifunctional biomass fuelled stove mainly comprises of two parts i.e. the stove and the combustion chamber. The manufactured stove has the option to use the stove in two different modes i.e. (i) using both the upper chamber and the stove for multifunctional or multiple pot applications or (ii) using only the stove for single pot operation. Thus BIS approved tests were conducted to determine the performance of the multifunctional biomass fuelled stove for both the modes of operation.

Another feature of the stove enables it to vary its air flow rate which further changes its power delivery rate. However according to BIS test procedure, with changes in the power delivery rate the water content needs to be changed. Therefore each mode is further tested for six categories of water content i.e. 2, 2.8, 3.7, 4.8, 6.1 and 7.7 kg which acts as thermal load during stove operations [24].

During the tests, the use of upper chamber improved the air flow rate which could be varied between 1.79×10^{-3} m^3/s and 7.55×10^{-3} m^3/s even with lower stove power output ranging between 2.29 kW to 5.31 kW. This has enabled better combustion, high flame temperature and higher heat transfer to the pot side wall from both flame and flue gas. As already discussed the multifunctional biomass fuelled stove forms an enclosed structure with the use of upper chamber which therefore enables a higher degree of air preheating and lower loss of heat from the flame to the surrounding. The stove operated with average efficiency of 34.60%, 34.47%, 34.80%, 36.62%, 37.62% and 33.39% for loads of 2, 2.8, 3.7, 4.8, 6.1 and 7.7 kg water respectively as in Fig. 4.9 on using upper chamber along with stove. Whereas without upper chamber the stove operated at

comparatively lower efficiency of 30.38%, 23.96%, 23.44%, 26.48%, 26.87% and 28.78% for loads of 2, 2.8, 3.7, 4.8, 6.1 and 7.7 kg water respectively as in Fig. 4.9. The above results thus validate the results obtained from the steady state heat transfer modeling of multifunctional biomass fuelled stove as discussed in Section 4.4.1.

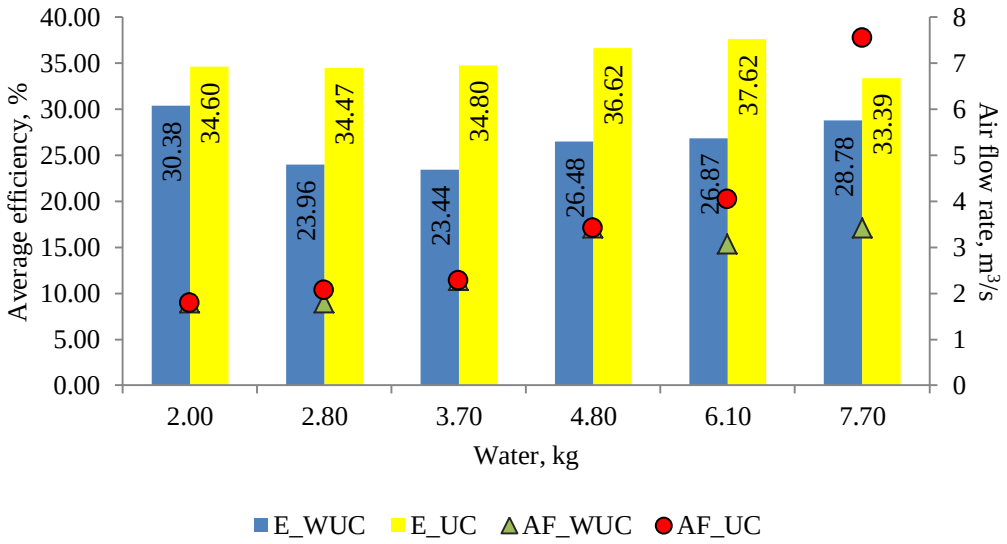

Fig.4.9: Variation in efficiency (E) and air flow rate (AF) with changes in water content for tests with (UC) and without (WUC) using upper chamber according to BIS test protocol

The tests without using the upper chamber showed lower standard deviations of 0.66%, 0.84%, 0.65%, 1.02%, 2.29% and 0.67% as compared to tests using upper chamber which showed standard deviations of 0.68%, 2.25%, 1.30%, 1.61%, 1.62% and 3.51% for loads of 2, 2.8, 3.7, 4.8, 6.1 and 7.7 kg water, respectively as in Fig. 4.10 and Eq. 4.46. The standard errors were lower for both the modes which ranged between 0.38% and 1.32% for tests without upper chamber and between 0.39% and 1.57% for tests using upper chamber with the stove as per Eq. 4.47. Fractional uncertainty also were lower for both the modes which ranged between 1.26×10^{-2} % and 4.93×10^{-2} % for tests without upper chamber and between 1.13×10^{-2} % and 4.71×10^{-2} % for tests using upper chamber with the stove as per Eq. 4.48.

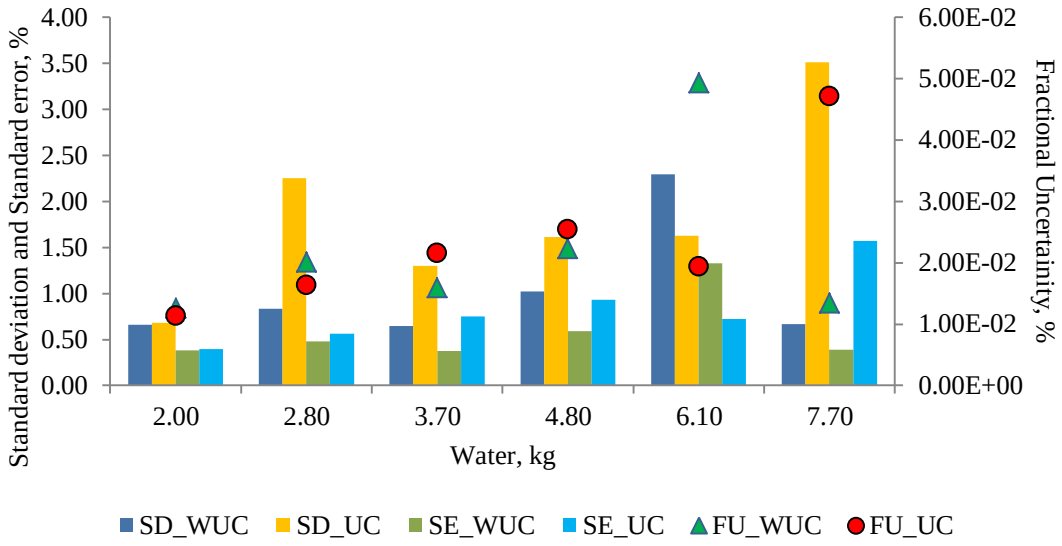

Fig.4.10: Variation in standard deviation (SD), standard error (SE) and fractional uncertainty (FU) with changes in water content with (UC) and without (WUC) using Upper Chamber for MBFS according to BIS test protocol

4.4.2.2 Water Boiling Test results

The multifunctional biomass fuelled stove is further tested using standard Water Boiling Test for biomass cook stove. The test includes three phases i.e. high power cold start phase, high power hot start phase and low power simmering test. During all the test phases uniform fuel size of $2\times2\times10^{-6}$ m^3 having net calorific value of 18.31 MJ/kg and moisture content of 10% is used. Loads of 5 liters water is used for both cold and hot start phases. Thermocouples and digital weighing balance were used during the test for measurements of temperature and weight respectively. The stove took 30 and 28 minutes with burning rates of 10.7 and 10.3 g/min to boil 5 liters of water during cold and hot start respectively as in Table 4.4. However the stove operates at highest efficiency of 45% during low power simmering test followed by 42% and 38% during high power hot start and cold start respectively. It could be observed that the multifunctional biomass fuelled stove shows suitability for low power simmering cooking as it operates at a lower burning rate of 5.4 g/min with output power of only 1.52 kW. The power output is comparatively higher during cold and hot start phases of 3.28 and 3.15 kW respectively. The stove also operates at a higher turn down ratio of 2.18 which shows the ability of the multifunctional biomass fuelled stove to vary its

power output for a larger range. This makes the multifunctional biomass fuelled stove suitable for a wider range of cooking variations.

Table 4.4: Average results of Water Boiling Test

Parameter	Unit	High power test (cold start)	High power test (hot start)	Low power test (simmering)
Time to boil Pot #1	min	30	28	
Temperature corrected time to boil Pot#1	min	32	30.2	
Burning rate	g/min	10.7	10.3	5.4
Thermal efficiency	%	38%	42%	45%
Specific fuel consumption	g/liter	62	55.4	46.9
Temperature corrected specific consumption	g/liter	66.3	59.2	
Firepower	W	3278	3155	1522
Turn down ratio				2.18

A total of three tests were conducted on the multifunctional biomass fuelled stove to determine the average values of performance as in Table 4.4. However uncertainties and errors could not be nullified. The determination of efficiency of the multifunctional biomass fuelled stove during WBT tests shows standard deviations of 1.73%, 1% and 2% respectively during cold start, hot start and simmering test phases respectively using Eq. 4.46. Thus the results obtained during simmering test shows a wider spread followed by cold start and hot start tests. Lower standard errors of 1%, 0.58% and 1.15% using Eq. 4.47 as well as fractional uncertainties of 2.63×10^{-2}, 1.37×10^{-2} and 2.57×10^{-2} using Eq. 4.48 were obtained during cold start, hot start and simmering test respectively as in Fig. 4.11.

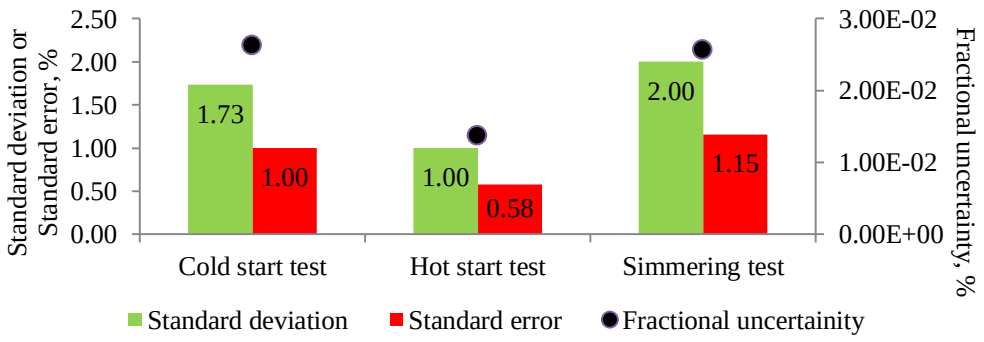

Fig. 4.11: Variation in standard deviation, standard error and fractional uncertainty with changes in phases during WBT test

4.4.3 Comparative performance analysis

The experimental results therefore shows that according to BIS for single pot operation the multifunctional biomass fuelled stove operates at 37.62% with power output of 4.5 kW whereas SHTM shows that it operates at 38.63% with power output of 4.5 kW. The stove is further tested using WBT by using the upper chamber for multiple pot cooking. According to WBT for multiple pots cooking the experimental results shows that the stove operates at 38% during cold start, 42% during hot start and 45% during simmering phases with power delivery of 3.28 kW, 3.15 kW and 1.52 kW respectively as in Fig. 4.12. Thus the average experimentally determined efficiency of multifunctional biomass fuelled stove is 42% during WBT. The SHTM on the other hand predicted that the stove will operate at an efficiency of 44.77% during multiple pots cooking according to WBT.

It is therefore observed that the SHTM could successfully predict the performance of the multifunctional biomass fuelled stove with lower deviations from experimentally obtained results. Thus the developed SHTM is validated for multifunctional biomass fuelled stove.

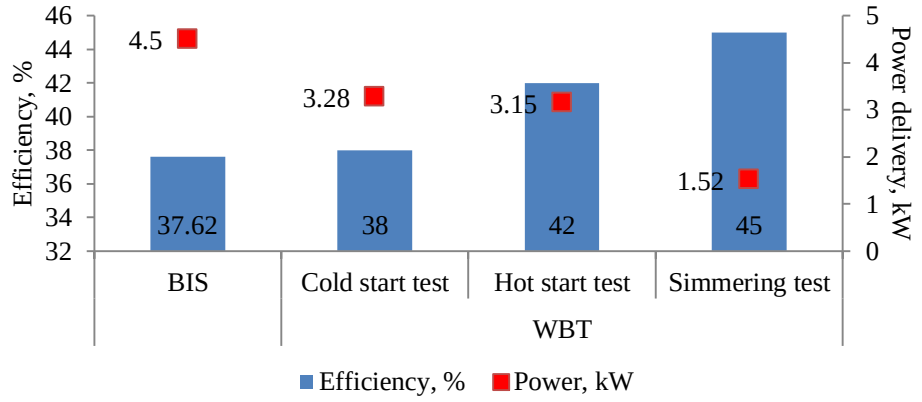

Fig.4.12: Experimental performance test results of multifunctional biomass fuelled stove

4.5 Summary

A multifunctional biomass fuelled stove with combustion air pre-heating and flue gas heat extraction is designed, modeled and developed in continuation of the present research work. The stove layout addresses some critical parameters and sections to

maximize heat utilization and minimizing losses using processes and functions as listed below:

1. Utilizing the combined process of flue gas heat extraction and reheating to preheat air and perform multifunctional activities or multiple pot cooking
2. Use of a counter-flow heat exchanging arrangement of spiral flow flue gas heat extractor, parallel flow flue gas heat extractor, parallel flow air preheater and radial flow air preheater, for flue gas heat extraction
3. Reduced thermal mass by creation of air separation between the upper chamber and stove
4. High portability and stability
5. Use of annular ring as flue gas collector as well as pot skirt
6. Enclosed flame and flue gas reduces heat loss
7. Forced draft for enhanced combustion efficiency and power variation, as well as induced draft for high flue gas heat extraction

The design thus developed is further analyzed for its performance prior to prototype development using Steady State Heat Transfer Modeling (SHTM) technique. The SHTM model varies with previously discussed model as the applicable designs and processes vary with change in stove design and configuration. The SHTM identifies 31 different stove heat transfer processes and determines efficiencies both according to BIS test and WBT. Highest instantaneous heat is trapped in charcoal produced during the steady state consideration i.e. 1853.64 W. SHTM shows that the design has the potential to recover 25.31% of waste heat from a system of 4.5 kW Multifunctional biomass fuelled stove and could be operated at BIS test efficiency of 38.63% for single pot operations and 44.77% during WBT for multiple pot operations. The results are satisfactory as they are above the required standards. A prototype of multifunctional biomass fuelled stove is further developed and tested using standard BIS and WBT procedures. Experimental laboratory tests shows that the stove could be operated at a highest single pot efficiency of 37.62% releasing 4.5 kW according to BIS test procedure. However during multiple pot operations WBT shows that the stove could be

operated at efficiencies of 38%, 42% and 45% during cold start, hot start and simmering test. The developed technology for multifunctional stove is applied for Indian Patents with application no.: 201831009091 and titled “Multifunctional Multiple Pot Solid Fuelled Stove with Combustion Air Pre-heating and Flue Gas Heat Extraction”.

Further feasibility for transfer of the technology involved in multipurpose stove is analyzed through determination of activities completed for technology transfer process, comparative analysis with other commercially available stoves and techno-economic analysis. A detailed study is presented in the following chapter.

REFERENCES

[1] *Eurostat news release, Production and consumption of wood in EU 27*. Retrieved on 5 Sep. 2017 from http://ec.europa.eu/eurostat/documents/2995521/5152954/5-29112012-AP-EN.PDF/727fab5c-46ba-408e-8d5d-0247e8ea6436?version=1.0, November, 2012.

[2] Bernelov, J. H., and Bernelov, E. I. *Wood burning stove with economizer*. US4738241, US Grant, 1986. Retrieved on 15 June 2017 from https://patents.google.com/patent/US4738241A/en?oq=US4738241, 1986.

[3] Teal, W. J. *Heat exchanger for furnace flue*. US5944090, US Grant, 1998. Retrieved on 15 June 2017 from https://patents.google.com/patent/US5944090A/en?oq=US5944090, 1998.

[4] Schwartz, L. A., Geiter, R., and Albertsen, P. S. *Catalytic stove*. US4319556, US Grant, 1981. Retrieved on 15 June 2017 from https://patents.google.com/patent/US4319556A/en?oq=US4319556, 1981.

[5] Kumar, M., Kumar, S., and Tyagi, S. K. Design, development and technological advancement in the biomass cookstoves: A review. *Renewable and Sustainable Energy Reviews*, 26: 265-285, 2013.

[6] Guo, B., Li, D., Cheng, C., Lü, Z. A., and Shen, Y. Simulation of biomass gasification with a hybrid neural network model. *Bioresource Technology*, 76(2): 77-83, 2001.

[7] Brown, D., Fuchino, T., and Maréchal, F. Solid fuel decomposition modelling for the design of biomass gasification systems. In *Computer Aided Chemical Engineering*, 21: 1661-1666, 2006.

[8] Pletcher, R. H., Tannehill, J. C., and Anderson, D. *Computational fluid mechanics and heat transfer*. CRC Press, Florida, 2012.

[9] Marklund, M., Tegman, R., and Gebart, R. CFD modelling of black liquor gasification: Identification of important model parameters. *Fuel*, 86(12-13): 1918-1926, 2007.

[10] Huiyun, Z. *Multi-functional energy-conserving firewood stove of movable*. CN206419985U, CN grant, 2017. Retrieved on 15 Mar. 2019 from https://patents.google.com/patent/CN206419985U/en?oq=CN206419985U, 2017.

[11] Murty, J. S., Khuntia, S., and Ray, H. *A multi-purpose stove useful for cooking, baking, space heating and drying*. 1114/DEL/1998. Retrieved on 14 Mar. 2018 from http://www.allindianpatents.com/patents/215495-a-multi-purpose-stove-useful-for-cooking-baking-space-heating-and-drying, 2008.

[12] Biao, S. *Dual purpose heating stove of cooking and hydrologic cycle*. CN206377698(U), CN Grant, 2017. Retrieved on 15 Mar. 2019 from https://patents.google.com/patent/CN206377698U/en?oq=CN206377698+U, 2017.

[13] Bharatbhai, P. *Portable stove.* 3568/MUM/2014, Indian Patent, 2016. Retrieved on 15 Mar. 2019 from http://ipindiaservices.gov.in/PatentSearch/PatentSearch//ViewApplicationStatus, 2016.

[14] Gogoi, B., and Baruah, D. C. *Multifunctional multiple pot solid fuelled stove with combustion air pre-heating and flue gas heat extraction.* 201831009091, 2019. Retrieved on 15 May 2019 from https://ipindiaservices.gov.in/PublicSearch/PublicationSearch/PatentDetails, 2019.

[15] Morini, G. L. Thermal characteristics of slug flow in rectangular ducts. *International journal of thermal sciences*, 38(2): 148-159, 1999.

[16] Sartori, E. Convection coefficient equations for forced air flow over flat surfaces. *Solar Energy*, 80(9): 1063-1071, 2006.

[17] Saastamoinen, J.J., Taipale, R., Horttanainen, M., and Sarkomaa, P. Propagation of the ignition front in beds of wood particles. *Combustion and flame*, 123(1-2): 214-226, 2000.

[18] Leuenberger, H. and Person, R. A. *Compilation of radiation shape factors for cylindrical assemblies*. American Society of Mechanical Engineers, New York, 1994.

[19] Pastor Ferrer, E., Rigueiro, A., Zárate López, L., Gimenez, A., Arnaldos Viger, J., and Planas Cuchi, E. November. Experimental methodology for characterizing flame emissivity of small scale forest fires using infrared thermography techniques. In *IV International Conference on Forest Fire Research 2002 Wildland Fire Safety Summit*, 1-11, 2002.

[20] Kausley, S. B., and Pandit, A.B. Modelling of solid fuel stoves. *Fuel*, 89(3): 782-791, 2010.

[21] Rohsenow, W. M. Technical Report No. 5: A method of correlating heat transfer data for surface boiling of liquids. Cambridge, Mass.: MIT Division of Industrial Cooperation, 1951.

[22] Welker, J. R., and Sliepcevich, C. M. Heat Transfer by Direct Flame Contact Fire Tests. Phase I. *National Academy of Sciences Washington DC Committee on Hazardous Materials*, 1971.

[23] Incropera, F. P. and Dewitt, D. P. *Fundamentals of heat and mass transfer*, Wiley-India Edition, 5th edition, 2009.

[24] Indian standard, Portable Solid Bio-mass Cookstove (chulha) (First revision) IS 13152 (Part 1): 2013, Bureau of Indian Standards, Aug. 2013. Retrieved on 23 Apr. 2016 from http://www.newdawnengineering.com/website/library/Stoves/Stove%20 Testing /Testing% 20Protocols/India/BIS%20stove%20test%20Feb%202014.pdf, February 2014.

[25] The Water Boiling Test, Version 4.2.3, Cookstove Emissions and Efficiency in a controlled Laboratory Setting, March, 2014. Retrieved on 15 Mar. 2017 from https://www.cleancookingalliance.org/binary-data/DOCUMENT/file/000/000/399-1.pdf, 2014.

[26] Measurements and error analysis, College Physics Labs Mechanics, The University of North Carolina, Chapel Hill. Retrieved on 22 April, 2020 from https://www.webassign.net/question_assets/unccolphysmechl1/measurements/manual.html